Photonic Topological Spin Pump in Synthetic Frequency Dimensions

Joseph Suh[,1] Gyunghun Kim[,1] Hyungchul Park,[1] Shanhui Fan,[2] Namkyoo Park[,3,*] and Sunkyu Yu[1,†]

[1]*Intelligent Wave Systems Laboratory, Department of Electrical and Computer Engineering,*
Seoul National University, Seoul 08826, Korea
[2]*Department of Electrical Engineering, Ginzton Laboratory, Stanford University, Stanford, California 94305, USA*
[3]*Photonic Systems Laboratory, Department of Electrical and Computer Engineering, Seoul National University,*
Seoul 08826, Korea

Reducing geometrical complexity while preserving desired wave properties is critical for proof-of-concept studies in wave physics, as evidenced by recent efforts to realize photonic synthetic dimensions, isospectrality, and hyperbolic lattices. Laughlin's topological pump, which elucidates quantum Hall states in cylindrical geometry with a radial magnetic field and a time-varying axial magnetic flux, is a prime example of these efforts. Here we propose a two-dimensional dynamical photonic system for the topological pumping of pseudospin modes by exploiting synthetic frequency dimensions. The system provides the independent control of pseudomagnetic fields and electromotive forces achieved by the interplay between mode-dependent and mode-independent gauge fields. To address the axial open boundaries and azimuthal periodicity of the system, we define the adjusted local Chern marker with rotating azimuthal coordinates, proving the nontrivial topology of the system. We demonstrate the adiabatic pumping for crosstalk-free frequency conversion with wave front molding. Our approach allows for reproducing Laughlin's thought experiment at room temperature with a scalable setup.

The quantum Hall effect represents one of the most important effects in topological physics, with potential applications for achieving backscattering-suppressed wave transport through disorder [1–4]. Laughlin's argument [5,6], which is based on gauge transformation and describes quantized conductance [7,8] through the adiabatic pumping of wave functions, represents an important milestone in the understanding of quantum Hall effects. Laughlin's model is composed of a cylinder subjected to a radial magnetic field B_ρ and an adiabatically varying axial magnetic flux $\Phi_z(t)$ that induces an electromotive force (EMF). Given its theoretical importance, it is certainly of interest to directly implement this model. However, the intrinsic geometry of the cylinder necessitates a three-dimensional (3D) platform, complicating its experimental realization. One of the intriguing approaches to address such a geometrical challenge is the implementation of 3D or even higher-dimensional systems and Hamiltonians in physical systems with lower geometrical dimensions [9–11], as shown in the realization of topological phenomena in non-Euclidean geometry [12] and quasicrystals [13]. Using this approach, demonstrating Laughlin's pump by emulating the axial transport on a cylindrical surface with a radial transport on a disk was achieved in [14,15].

The concept of synthetic frequency dimensions [16] has provided new design freedom in addressing the geometrical challenge of Laughlin's pump [5]. By introducing intermodal coupling via spatiotemporal modulation, a synthetic frequency dimension can be realized through the coupling of modes with different frequencies, resulting in dynamics along a frequency axis. In this way, higher-dimensional physics can be reproduced with experimentally accessible lower-dimensional platforms. Synthetic dimensions have been used in the study of topological phenomena [17–22], quantum computing [23,24], and matrix-vector multiplications [25]. In a cold-atom system, Laughlin's pump in synthetic dimensions was implemented recently with very few spin states for the azimuthal axis [26]. However, it remains a challenge to achieve pumping operations at room temperature with geometrical scalability beyond the limited number of spin states. Given the demonstrated potential of synthetic dimensions in photonics—evidenced by the experimental realization of tunable pseudomagnetic fields in ladders using a single resonator [27]—suitable photonic systems could tackle the geometrical complexities of Laughlin's pump while ensuring a room-temperature and scalable configuration.

Here we propose a photonic realization of Laughlin's pump. In our realization, the axial dimension of the cylindrical geometry in Laughlin's pump is implemented in the synthetic dimension. Our realization enables the creation of pseudomagnetic fluxes of B_ρ and $\Phi_z(t)$ as well as their independent control, which is essential for Laughlin's pump. We demonstrate adiabatic pumping in the synthetic dimension with designed light injections, which allows for crosstalk-free frequency conversion of light as

well as the molding of spatial profiles. To examine the nontrivial topological nature of the cylinder, we introduce the adjusted local Chern marker, which clarifies the origin of the adiabatic pumping rate of the system. Our implementation is the first study of bulk topological dynamics on Laughlin cylinder using integrated photonic platforms, achieving scalable geometry.

Hardware implementation.—Laughlin's pump is implemented with a radial magnetic field and an EMF from an axial magnetic flux [28] [Fig. 1(a)]. It is well known that the necessary field and EMF can be achieved by employing the gauge field $\mathbf{A}(z,t) = [-B_\rho z + \Phi_z(t)/2\pi\rho]\boldsymbol{\varphi}$ [29], as $(\nabla \times \mathbf{A}) \cdot \boldsymbol{\rho} = B_\rho$ and $\partial_t \oint \mathbf{A} \cdot d\mathbf{l} = \partial_t \Phi_z(t)$, where $d\mathbf{l}$ denotes the φ-axis infinitesimal length. In an ultracold atom system [26], the gauge field was realized with the momentum exchange in two-photon transitions and the
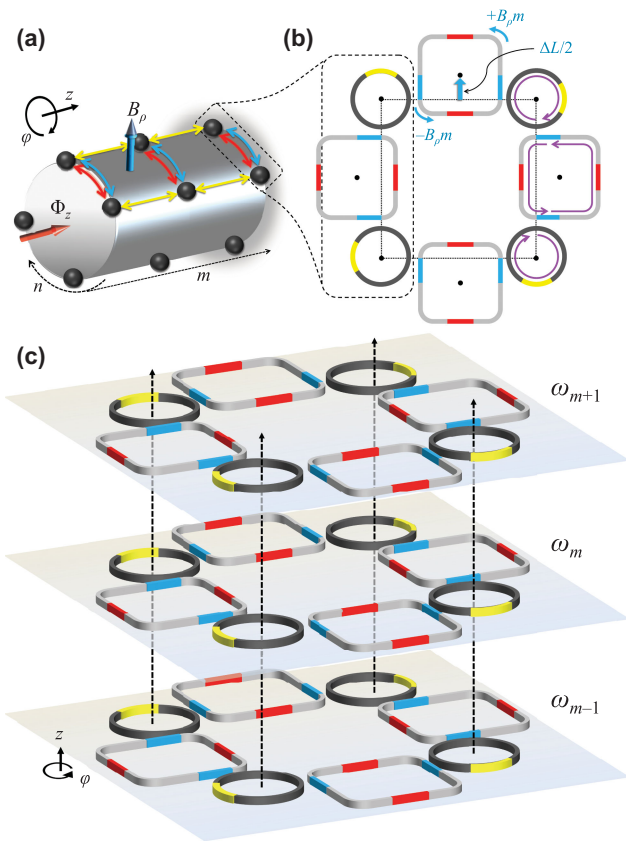

FIG. 1. Photonic hardware for topological spin pumps. (a) Schematic of the pump. Each site for a resonance mode is labelled by the indices $m \in [1, M]$ and $n \in [1, N]$, where M and N are the numbers of the modes and resonators, respectively. Colored arrows indicate the coupling. (b) Coupled-resonator platform for realizing (a). Black circles and gray curved squares denote resonators and waveguide loops, respectively. The red and yellow regions are tunable phase shifters for the loops and resonators, respectively. Purple arrows show wave circulations. Blue regions indicate structural imbalance. (c) Layers of coupled resonators along the synthetic axis. ω_m is the mth-mode resonance frequency.
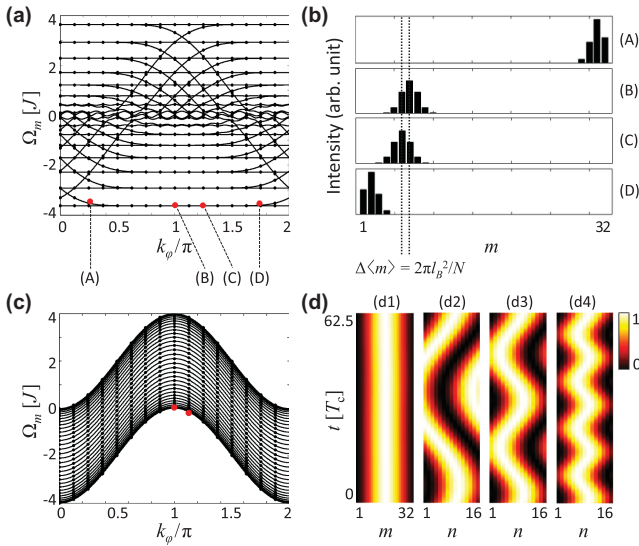
relative phase difference of laser fields involved in $\pm\boldsymbol{\varphi}$ hopping.

We emulate Laughlin's pump by achieving the necessary time-reversal symmetry breaking for topological phenomena effectively with one of the pseudospin modes: clockwise traveling-wave resonances. The magnetic fluxes of the pump are implemented through the pseudogauge field $\mathbf{A}$, extending two-dimensional (2D) topological photonics [30,31] to the cylindrical geometry defined with the synthetic dimension. Figure 1 illustrates the resonator-based implementation of Laughlin's pump. Each point of the space-mode ($\varphi - z$) cylindrical coordinate corresponds to an individual resonance. The arrows connecting points represent the spatial (φ-axis) and intermodal (z-axis) coupling. We utilize nonresonant waveguide loops as the spatial couplers between resonators, which have been employed in realizing gauge fields [30,32]. The couplers are assumed to have a length $L_{\rm w}$, obtaining the phase evolution of $[4(m + m_0) + 1]\pi$ per circulation for the mth resonance mode, where m_0 is a sufficiently large integer for the offset. As demonstrated in 2D planar structures [30,32], the couplers allow for space-mode hopping with the desired gauge field $\mathbf{A}$, while maintaining destructive interferences within the couplers.

In the proposed platform, we achieve $\Phi_z(t)$, the synthetic z axis, and B_ρ as follows. First, employing the method of realizing magnetic fluxes across a 2D plane [30,33], we derive the EMF $\partial_t \Phi_z(t)$ from the dynamic gauge $A_{\rm D}(t) = \Phi_z(t)/2\pi\rho$ by applying the time-varying modulation of the coupling phase [red regions in Fig. 1(b)]. While applying the opposite perturbations in the upper and lower arms to maintain the nonresonant condition, we utilize time-varying phase shifters [34,35], which are set to assign $\eta(t)$ phase evolutions to the modes of interest. The phase evolutions derive $A_{\rm D}(t) = \eta(t)$, which is mode independent around the mode number m within the linear dispersion regime (note S1 in the Supplemental Material [36]).

Second, we implement the synthetic z axis following the method in previous studies [37,44]: employing spatiotemporally varying modulations within resonators [yellow regions in Fig. 1(b)] to achieve intermodal coupling. Hopping amplitudes along the φ and z axes are set to be equal, and there is no additional phase shift along the z axis.

Finally, the static gauge field $A_{\rm S}(z) = -B_\rho z$ corresponds to the coupling phases linear to mode numbers. To achieve $A_{\rm S}(z)$, we introduce the structural imbalance in the upper and lower arms by introducing the dislocation $\Delta L/2$ [blue regions in Fig. 1(b)]. Each mode experiences different path lengths for the imbalance and the following gauges, which leads to m-dependent hopping phase difference $\pm[4(m + m_0) + 1]\pi\Delta L/L_{\rm w}$ and the consequent magnetic field $B_\rho = -4\pi\Delta L/L_{\rm w}$. Such a B_ρ field has been experimentally demonstrated in [27] with two pseudospin modes. To realize the cylindrical geometry of Laughlin's pump, we extend the prior work to implement the B_ρ field

FIG. 2. Band properties of pseudospin pumps with either B_ρ or $\partial_t \Phi_z(t)$. (a) Pump spectrum with $A_D(t) = 0$ for $B_\rho = \pi/8$, $M = 32$, and $N = 16$. (b) Eigenfunction intensities along the frequency ($m-$) axis. (c) Pump spectrum with $B_\rho = 0$ for $A_D(t) = 0$. (d) Temporal evolution of the beam profiles on the cylinder according to linearly varying $A_D(t)$. An initial wave packet is a superposition of two adjacent eigenfunctions in the lowest band [red dots in (c)]. $T_c = 8/J$ is the characteristic time.

for a larger number of resonators. Although introducing the structural imbalance for $A_S(z)$ is similar to $A_D(t)$ in terms of achieving gauge fields, the critical difference is that $A_D(t)$ is designed to be m independent.

Our construction allows independent control of a pseudomagnetic field and flux through structural and temporal modulations, completing the implementation of Laughlin's pump for pseudospin modes in the synthetic dimension. The Hamiltonian of the system is given by (note S1 in [36]):

$$H = -J\left(\sum_z \sum_{(\varphi_1,\varphi_2)\in\Lambda_\varphi} e^{i[A_s(z)+A_D(t)]} a^\dagger_{z,\varphi_2} a_{z,\varphi_1}\right.$$
$$\left. + \sum_{(z_1,z_2)\in\Lambda_z} \sum_\varphi a^\dagger_{z_2,\varphi} a_{z_1,\varphi}\right) + \text{H.c.,} \qquad (1)$$

where J is the hopping amplitude between nearest neighbors (NNs) in the $\varphi - z$ coordinate, $a_{z,\varphi}$ (or $a^\dagger_{z,\varphi}$) is the annihilation (or creation) operator at the site (z,φ), Λ_z (or Λ_φ) is a set of NN pairs along the z (or φ) axis, and H.c. is the Hermitian conjugate. Assuming the adiabatic change of $A_D(t)$, the instantaneous band $\Omega_m(k_\varphi)$ can be obtained, where $m \in [1, M]$ and k_φ is the discretized quasimomentum from φ periodicity.

Pseudomagnetic fields and EMFs.—Before exploring the interplay of B_ρ and $\partial_t \Phi_z(t)$, we examine their separate impacts. First, we consider the scenario where

$A_D(t) = 0$ and B_ρ is static: only the mode-dependent gauge $[A_S(z) = -B_\rho z]$ exists. This system corresponds to the modified Hofstadter model with a finite and rotationally symmetric structure [45]. Figure 2(a) illustrates the band diagram of the system obtained from Eq. (1). We set a pseudomagnetic flux per plaquette by B_ρ to be $\pi/8$, which ideally leads to the Chern number of 1 to each magnetic Bloch band at the 7 lowest eigenenergies [46] in the thermodynamic limit. The magnetic Bloch bands comprising Landau levels support the eigenfunctions with the z centers of $k_\varphi l_B^2$ [(B) and (C) in Figs. 2(a) and 2(b)], where l_B is the magnetic length $(1/B_\rho)^{1/2}$ [28]. The finite length of the cylinder along the synthetic z axis results in topologically protected edge states crossing the gaps [4,20]. In the synthetic frequency dimension, the existence of edge states corresponds to the maintenance of either the lowest or highest resonance frequencies despite intermodal coupling [(A) and (D) in Figs. 2(a) and 2(b)].

Second, we consider the system where $B_\rho = 0$; only the mode-independent gauge field $A_D(t)$ exists. The system with $B_\rho = 0$ is topologically trivial, and thus, the Bloch band becomes sinusoidal with respect to k_φ [Fig. 2(c)]. Because of gauge transformation [29], $A_D(t)$ applied to this topologically trivial system leads to the band shift along the k_φ axis, which corresponds to the intraband transition when the band diagram remains fixed. The constant EMF $\partial_t \Phi_z(t)$ with linearly varying $A_D(t)$, which corresponds to the electric field along the azimuthal axis, results in Bloch oscillations [Fig. 2(d)]. As widely studied [47,48], the angular frequency $|\partial_t A_D(t)|$ and amplitude $2J/|\partial_t A_D(t)|$ of the oscillation are determined by the slope of $A_D(t)$ [(d2–d4) in Fig. 2(d)], while the z centers remain constant [(d1) in Fig. 2(d)].

Local Chern marker.—Because the modes participating in the synthetic dimension are constrained by the natural boundary originating from the group velocity dispersion (GVD) [49,50], the proposed pump geometry is inherently finite. Such finite systems impede the direct use of the Chern number defined under the periodic boundary condition. Therefore, we employ an alternative measure: local Chern marker [51]. This marker, approaching the Chern number through the integration across the infinite crystalline structure, serves as a useful local measure that captures the topological features of the bulk, even in finite-size samples. Therefore, comparing the local Chern marker in the bulk with the ideal Chern number allows for examining the validity of the synthetic axis length for the analogy of Laughlin's pump. In discussing topological properties, we assume sharp boundaries along the synthetic dimension achievable with abrupt changes in the GVD [49] or the coupling with auxiliary rings [25,38].

The local Chern marker $C_L(\mathbf{r}_{mn})$ is defined as [51]

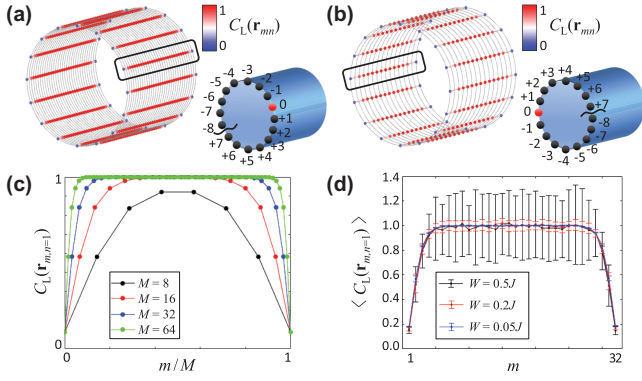$$C_L(\mathbf{r}_{mn}) = 2\pi i \langle \mathbf{r}_{mn} | [PmP, PnP] | \mathbf{r}_{mn} \rangle, \qquad (2)$$

FIG. 3. Real-space topological measures. (a),(b) Coordinate-indexing scheme and the lowest-band $C_L(\mathbf{r}_{mn})$ for (a) $M = 32$ and (b) $M = 16$. (c) $C_L(\mathbf{r}_{mn})$ as a function of m/M for different M. (d) The averages and standard deviations of $C_L(\mathbf{r}_{mn})$ for 100 random realizations for each W, where W denotes the degree of diagonal disorder uniformly distributed over $[-W, +W]$. The error bars are 10 times the standard deviations for clarity.

where $|\mathbf{r}_{mn}\rangle = (m, n)$ is the discretized position state on the $z - \varphi$ cylinder surface of Fig. 1(a), and P is the Fermi projection operator to the valence band [52]. The projected operators PmP and PnP originate from remedying ill-defined position operators in the real-space representation of Chern number and the modern theory of polarization.

Although $C_L(\mathbf{r}_{mn})$ is defined for a 2D plane, our synthetic-dimensional system has cylindrical geometry with axial open boundaries and azimuthal periodicity. Therefore, we redefine the index set of n in calculating $C_L(\mathbf{r}_{mn})$, as $\{n\} = \{\ldots, -2, -1, 0, +1, +2, \ldots\}$, where we set an index n for the pth element to zero [a subset of Figs. 3(a) and 3(b)]. This rotating coordinate guarantees the local continuity of the azimuthal position near $\mathbf{r}_{mp}$, which is necessary for reflecting the periodicity of the cylinder. Although such a configuration breaks the trivial condition of global topology for open-boundary systems, the non-trivial feature at each local position is preserved because the position discontinuity does not affect the nearsighted operator P in evaluating $C_L(\mathbf{r}_{mp})$ [51,53].

Figures 3(a) and 3(b) show the distribution of $C_L(\mathbf{r}_{mn})$ for the lowest band with different values of M. While the ideal Chern number with $M \to \infty$ is 1 with $B_\rho = \pi/8$, the local Chern marker within the bulk has a near unity value, demonstrating the validity of the local Chern marker. Because of the broken translational symmetry, the value of $C_L(\mathbf{r}_{mn})$ decreases near the boundary [Figs. 3(a)–3(d)]. Figure 3(c) demonstrates that $C_L(\mathbf{r}_{mn})$ serves as a well-defined local quantity to examine the valid range of our model ($M \geq 16$) as an approximation of the ideal Laughlin's pump. $C_L(\mathbf{r}_{mn})$ is robust to diagonal disorder, demonstrating the noise immunity of the pump [Fig. 3(d)].

Adiabatic pumping.—Based on Fig. 3, we investigate adiabatic pumping of topological edge states. We employ an external waveguide coupled to one of the resonators to
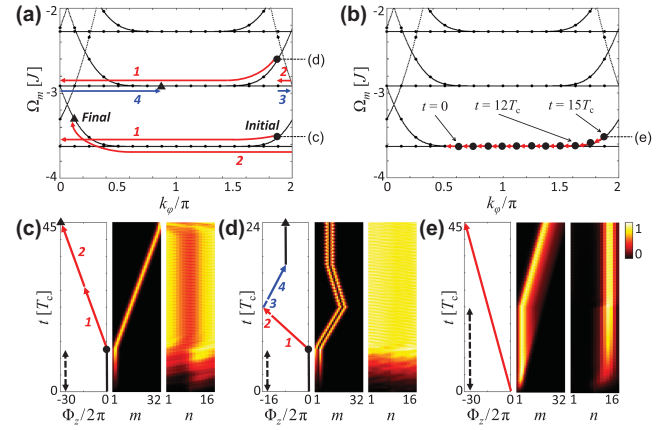
FIG. 4. Adiabatic pumping. Pumping dynamics in (a),(b) band diagrams and (c)–(e) the corresponding temporal monitoring of beam profiles: (c),(d) for (a) and (e) for (b). In (a),(c),(d), initial states (black circles) undergo adiabatic intraband transition due to $\Phi_z(t)$ and arrive at the final states (black triangles). In (b), black dots denote each excitation at the time t. The colored numbers of the lower ('1,2') and higher ('1–4') bands in (a) denote the sequences of the pumping in (c) and (d), respectively. In the left figures of (c)–(e), solid and dashed arrows represent $\Phi_z(t)$ and the temporal range of wave excitations, respectively. (b) shows the lowest band occupation after the simultaneous excitation of the incidence and pumping, which leads to spatial (n) localization in (e). The displacement along the frequency (m) axis [center figures in (c)–(e)] is proportional to $\Delta\Phi_z$. Nodeless single rails in (c),(e) and double rails with a node in (d) originate from the ground and first excited state excitations in (a),(b).

excite the edge state. The incident frequency is the reference frequency along the synthetic axis detuned with the eigenfrequency of the target edge state.

Figure 4 shows examples of adiabatic pumping with slowly varying $\Phi_z(t)$ for the temporally bounded wave excitations. The origin of this phenomenon is the adiabatic change of k_φ induced by $\partial_t \Phi_z(t)$, which results in the adiabatic intraband transition of edge states to bulk states [red and blue arrows in Fig. 4(a)]. Because the states are localized along the z axis around their k_φ-dependent centers $k_\varphi l_B^2$ [Fig. 2(b)], the intraband transition leads to the transport along the z axis [Figs. 4(c) and 4(d)]. After the transition to the bulk modes, the azimuthal group velocity $\partial\Omega_m/\partial k_\varphi$ becomes zero, maintaining the spatial profile inside the coupled resonator platform. The phenomena can be interpreted as the $\mathbf{E} \times \mathbf{B}$ drift in crystalline structures from the viewpoint of classical electrodynamics [46,54].

Because of the synthetic-dimensional configuration, the adiabatic pumping in our example corresponds to frequency conversion along the synthetic dimension. The separation of the wave excitation and EMF pumping in Figs. 4(a), 4(c), and 4(d) corresponds to the one-shot excitation of a topological band and its sequential pumping. Such an implementation leads to the localization in the reciprocal space [black circles in Fig. 4(a)], resulting in the

spatial broadening of the pumped mode. To achieve the spatial engineering of frequency-conversion functionality, we devise the configuration of filling the topological band by simultaneously applying the wave incidence and pumping [dashed and solid arrows in Fig. 4(e)]. This pumping technique enables the broadening in k_φ-axis [Fig. 4(b)], leading to spatial localization [Fig. 4(e)] while preserving frequency conversion functionality. Therefore, engineering incident waves allows for the designed excitation in the k_φ axis and the following spatial profiles in frequency conversion.

Importantly, the pumping example demonstrates the validity of local Chern markers in Fig. 3. The ratio of the normalized frequency drift $\Delta\langle m\rangle/(2\pi l_B^2/N)$ measured inside the bulk to the normalized magnetic flux change $\Delta\Phi_z/2\pi$ is close to unity in Fig. 4, which is theoretically identical to the Chern number [28]. This result is consistent with the local Chern marker $C_L(\mathbf{r}_{mn}) \sim 1$ in Fig. 3.

To explore the experimental feasibility, we perform numerical simulations in note S2 in [36], using standard parameters in integrated photonics of 1550 nm wavelength operations. By employing finite-difference time-domain simulations with Tidy3d [39,40], we show that the pump can be designed with acceptable system parameters [38,41–43]: a space-mode hopping near $J = 1.25$ GHz and 4π-range phase shifters, by applying a 100 nm coupling gap and $<1\%$ refractive index change. In light of the temporal ranges applied in Figs. 2 and 4, the obtained parameters align well with resonator quality factors of $\sim 10^6$; a feasible requirement for all-waveguide resonators [55] or fiber-ring systems [27] with electro-optic modulations [56]. Designing larger J alleviates the constraints on quality factors.

We also examine the valid range of crosstalk-free pump operations, by analyzing broken adiabaticity (note S3 in [36]), and the emergences of diagonal, spin-mixing (note S4 in [36]), and synthetic-dimensional disorder (note S5 in [36]). The results demonstrate topological natures of the spin pump; more robust pumping to diagonal disorder than spin-mixing disorder, in a similar context to the quantum spin Hall effect [30]. However, using both pseudospin modes may enable more multifaceted phenomena, such as Rashba interactions [57].

We have demonstrated the scalable photonic realization of a topological spin pump analogous to Laughlin's configuration by harnessing the synthetic dimension and time-varying gauge fields. By engineering dynamical gauges and resonances that were recently employed in programmable photonics [58], we develop the design strategy for B_ρ, $\Phi_z(t)$, and the synthetic z axis to realize the topological spin pump: the mode-dependent structural imbalance, mode-independent gauge fields, and spatiotemporal modulation of resonances. The platform allows for controlling the magnetic field and EMF independently in spatial and modal axes. By employing the local Chern marker, we proved that the suggested structure provides nontrivial topological features within finite spaces. The pumping examples illustrate substantial design freedom for frequency conversion, including the designed conversion trajectory with wave front engineering. Our proposal provides enhanced scalability because the spatial footprint relies solely on azimuthally arranged resonators. This synthetic-dimensional configuration using classical optic elements is more extendable than 2D topological platforms where the spatial footprint is determined by the discretization of the entire geometry [9,10,14], or a cold-atom Laughlin's pump with an azimuthal axis composed of limited spin states [26]. We also envisage that band filling through the sequential edge mode incidence and adiabatic pumping allows for classical realizations of quantized conductance and magnetic Bloch bands by imaging energy flows.

*Corresponding author: nkpark@snu.ac.kr
†Corresponding author: sunkyu.yu@snu.ac.kr

[1] Z. Wang, Y. Chong, J. D. Joannopoulos, and M. Soljačić, Reflection-free one-way edge modes in a gyromagnetic photonic crystal, Phys. Rev. Lett. **100**, 013905 (2008).

[2] B. Bahari, A. Ndao, F. Vallini, A. El Amili, Y. Fainman, and B. Kanté, Nonreciprocal lasing in topological cavities of arbitrary geometries, Science **358**, 636 (2017).

[3] Z. Yang, F. Gao, X. Shi, X. Lin, Z. Gao, Y. Chong, and B. Zhang, Topological acoustics, Phys. Rev. Lett. **114**, 114301 (2015).

[4] M. Z. Hasan and C. L. Kane, Colloquium: Topological insulators, Rev. Mod. Phys. **82**, 3045 (2010).

[5] R. B. Laughlin, Quantized Hall conductivity in two dimensions, Phys. Rev. B **23**, 5632 (1981).

[6] B. I. Halperin, Quantized Hall conductance, current-carrying edge states, and the existence of extended states in a two-dimensional disordered potential, Phys. Rev. B **25**, 2185 (1982).

[7] K. von Klitzing, G. Dorda, and M. Pepper, New method for high-accuracy determination of the fine-structure constant based on quantized Hall resistance, Phys. Rev. Lett. **45**, 494 (1980).

[8] D. J. Thouless, M. Kohmoto, M. P. Nightingale, and M. den Nijs, Quantized Hall conductance in a two-dimensional periodic potential, Phys. Rev. Lett. **49**, 405 (1982).

[9] M. Hafezi, Measuring topological invariants in photonic systems, Phys. Rev. Lett. **112**, 210405 (2014).

[10] S. Mittal, S. Ganeshan, J. Fan, A. Vaezi, and M. Hafezi, Measurement of topological invariants in a 2D photonic system, Nat. Photonics **10**, 180 (2016).

[11] W. Hu, J. C. Pillay, K. Wu, M. Pasek, P. P. Shum, and Y. Chong, Measurement of a topological edge invariant in a microwave network, Phys. Rev. X **5**, 011012 (2015).

[12] S. Yu, X. Piao, and N. Park, Topological hyperbolic lattices, Phys. Rev. Lett. **125**, 053901 (2020).

[13] Y. E. Kraus, Y. Lahini, Z. Ringel, M. Verbin, and O. Zilberberg, Topological states and adiabatic pumping in quasicrystals, Phys. Rev. Lett. **109**, 106402 (2012).

[14] B. Jeanneret, B. D. Hall, H.-J. Bühlmann, R. Houdré, M. Ilegems, B. Jeckelmann, and U. Feller, Observation of the integer quantum Halleffect by magnetic coupling to a Corbino ring, Phys. Rev. B **51**, 9752 (1995).

[15] M. Kawamura, M. Mogi, R. Yoshimi, T. Morimoto, K. S. Takahashi, A. Tsukazaki, N. Nagaosa, M. Kawasaki, and Y. Tokura, Laughlin charge pumping in a quantum anomalous Hall insulator, Nat. Phys. **19**, 333 (2023).

[16] L. Yuan, Q. Lin, M. Xiao, and S. Fan, Synthetic dimension in photonics, Optica **5**, 1396 (2018).

[17] T.-S. Zeng, C. Wang, and H. Zhai, Charge pumping of interacting fermion atoms in the synthetic dimension, Phys. Rev. Lett. **115**, 095302 (2015).

[18] J. H. Han, J. H. Kang, and Y. Shin, Band gap closing in a synthetic Hall tube of neutral fermions, Phys. Rev. Lett. **122**, 065303 (2019).

[19] C.-H. Li, Y. Yan, S.-W. Feng, S. Choudhury, D. B. Blasing, Q. Zhou, and Y. P. Chen, Bose-Einstein condensate on a synthetic topological Hall cylinder, PRX Quantum **3**, 010316 (2022).

[20] O. Zilberberg, S. Huang, J. Guglielmon, M. Wang, K. P. Chen, Y. E. Kraus, and M. C. Rechtsman, Photonic topological boundary pumping as a probe of 4D quantum Hall physics, Nature (London) **553**, 59 (2018).

[21] E. Lustig, S. Weimann, Y. Plotnik, Y. Lumer, M. A. Bandres, A. Szameit, and M. Segev, Photonic topological insulator in synthetic dimensions, Nature (London) **567**, 356 (2019).

[22] Q. Lin, X.-Q. Sun, M. Xiao, S.-C. Zhang, and S. Fan, A three-dimensional photonic topological insulator using a two-dimensional ring resonator lattice with a synthetic frequency dimension, Sci. Adv. **4**, 2774 (2018).

[23] U. A. Javid, R. Lopez-Rios, J. Ling, A. Graf, J. Staffa, and Q. Lin, Chip-scale simulations in a quantum-correlated synthetic space, Nat. Photonics **17**, 883 (2023).

[24] B. Bartlett, A. Dutt, and S. Fan, Deterministic photonic quantum computation in a synthetic time dimension, Optica **8**, 1515 (2021).

[25] S. Buddhiraju, A. Dutt, M. Minkov, I. A. D. Williamson, and S. Fan, Arbitrary linear transformations for photons in the frequency synthetic dimension, Nat. Commun. **12**, 2401 (2021).

[26] A. Fabre, J.-B. Bouhiron, T. Satoor, R. Lopes, and S. Nascimbene, Laughlin's topological charge pump in an atomic Hall cylinder, Phys. Rev. Lett. **128**, 173202 (2022).

[27] A. Dutt, Q. Lin, L. Yuan, M. Minkov, M. Xiao, and S. Fan, A single photonic cavity with two independent physical synthetic dimensions, Science **367**, 59 (2020).

[28] R. B. Laughlin, Nobel lecture: Fractional quantization, Rev. Mod. Phys. **71**, 863 (1999).

[29] J. K. Jain, *Composite Fermions* (Cambridge University Press, Cambridge, England, 2007).

[30] M. Hafezi, E. A. Demler, M. D. Lukin, and J. M. Taylor, Robust optical delay lines with topological protection, Nat. Phys. **7**, 907 (2011).

[31] K. Fang, Z. Yu, and S. Fan, Realizing effective magnetic field for photons by controlling the phase of dynamic modulation, Nat. Photonics **6**, 782 (2012).

[32] M. Hafezi, S. Mittal, J. Fan, A. Migdall, and J. M. Taylor, Imaging topological edge states in silicon photonics, Nat. Photonics **7**, 1001 (2013).

[33] T. Ozawa, H. M. Price, A. Amo, N. Goldman, M. Hafezi, L. Lu, M. C. Rechtsman, D. Schuster, J. Simon, O. Zilberberg, and I. Carusotto, Topological photonics, Rev. Mod. Phys. **91**, 015006 (2019).

[34] N. C. Harris, Y. Ma, J. Mower, T. Baehr-Jones, D. Englund, M. Hochberg, and C. Galland, Efficient, compact and low loss thermo-optic phase shifter in silicon, Opt. Express **22**, 10487 (2014).

[35] M. Notaros, T. Dyer, M. Raval, C. Baiocco, J. Notaros, and M. R. Watts, Integrated visible-light liquid-crystal-based phase modulators, Opt. Express **30**, 13790 (2022).

[36] See Supplemental Material at http://link.aps.org/supplemental/10.1103/PhysRevLett.132.033803 for (note S1) temporal coupled mode theory for tight-binding formulation, (note S2) full-wave simulation for system parameters, (note S3) validity of adiabatic modulations, (note S4) diagonal and spin-mixing disorder, (note S5) coupling disorder along the synthetic axis, which includes Refs. [12,30,37–43].

[37] A. Dutt, M. Minkov, Q. Lin, L. Yuan, D. A. B. Miller, and S. Fan, Experimental band structure spectroscopy along a synthetic dimension, Nat. Commun. **10**, 3122 (2019).

[38] A. Dutt, L. Yuan, K. Y. Yang, K. Wang, S. Buddhiraju, J. Vučković, and S. Fan, Creating boundaries along a synthetic frequency dimension, Nat. Commun. **13**, 3377 (2022).

[39] T. W. Hughes, M. Minkov, V. Liu, Z. Yu, and S. Fan, A perspective on the pathway toward full wave simulation of large area metalenses, Appl. Phys. Lett. **119**, 150502 (2021).

[40] See https://www.flexcompute.com for "Tidy3d".

[41] Q. Lin, M. Xiao, L. Yuan, and S. Fan, Photonic Weyl point in a two-dimensional resonator lattice with a synthetic frequency dimension, Nat. Commun. **7**, 13731 (2016).

[42] H. Jung, C. Xiong, K. Y. Fong, X. Zhang, and H. X. Tang, Optical frequency comb generation from aluminum nitride microring resonator, Opt. Lett. **38**, 2810 (2013).

[43] B. Ouyang, Y. Xing, W. Bogaerts, and J. Caro, Silicon ring resonators with a free spectral range robust to fabrication variations, Opt. Express **27**, 38698 (2019).

[44] Z. Yu and S. Fan, Complete optical isolation created by indirect interband photonic transitions, Nat. Photonics **3**, 91 (2009).

[45] D. R. Hofstadter, Energylevels and wavefunctions of Bloch electrons in rational and irrational magneticfields, Phys. Rev. B **14**, 2239 (1976).

[46] M.-C. Chang and Q. Niu, Berry phase, hyperorbits, and the Hofstadter spectrum, Phys. Rev. Lett. **75,** 1348 (1995).

[47] M. Ben Dahan, E. Peik, J. Reichel, Y. Castin, and C. Salomon, Bloch oscillations of atoms in an optical potential, Phys. Rev. Lett. **76,** 4508 (1996).

[48] Y. Ke, S. Hu, B. Zhu, J. Gong, Y. Kivshar, and C. Lee, Topological pumping assisted by Bloch oscillations, Phys. Rev. Res. **2,** 033143 (2020).

[49] L. Yuan, Y. Shi, and S. Fan, Photonic gauge potential in a system with a synthetic frequency dimension, Opt. Lett. **41,** 741 (2016).

[50] Q. Shan, D. Yu, G. Li, L. Yuan, and X. Chen, One-way topological states along vague boundaries in synthetic frequency dimensions including group velocity dispersion, Prog. Electromagn. Res. **169,** 33 (2020).

[51] R. Bianco and R. Resta, Mapping topological order in coordinate space, Phys. Rev. B **84,** 241106(R) (2011).

[52] N. Marzari, A. A. Mostofi, J. R. Yates, I. Souza, and D. Vanderbilt, Maximally localized Wannier functions: Theory and applications, Rev. Mod. Phys. **84,** 1419 (2012).

[53] W. Kohn, Density functional and density matrix method scaling linearly with the number of atoms, Phys. Rev. Lett. **76,** 3168 (1996).

[54] D. Xiao, M.-C. Chang, and Q. Niu, Berry phase effects on electronic properties, Rev. Mod. Phys. **82,** 1959 (2010).

[55] M. W. Puckett, K. Liu, N. Chauhan, Q. Zhao, N. Jin, H. Cheng, J. Wu, R. O. Behunin, P. T. Rakich, K. D. Nelson, and D. J. Blumenthal, 422 Million intrinsic quality factor planar integrated all-waveguide resonator with sub-MHz linewidth, Nat. Commun. **12,** 934 (2021).

[56] Y. Hu, C. Reimer, A. Shams-Ansari, M. Zhang, and M. Loncar, Realization of high-dimensional frequency crystals in electro-optic microcombs, Optica **7,** 1189 (2020).

[57] Y. A. Bychkov and E. I. Rashba, Oscillatory effects and the magnetic susceptibility of carriers in inversion layers, J. Phys. C **17,** 6039 (1984).

[58] X. Piao, S. Yu, and N. Park, Programmable photonic time circuits for highly scalable universal unitaries, arXiv:2305.17632.